Journal of Hydrology 369 (2009) 403–415

Contents lists available at ScienceDirect

Journal of Hydrology

journal homepage: www.elsevier.com/locate/jhydrol

Large scale nutrient modelling using globally available datasets: A test for the Rhine basin

Sibren Loos *, Hans Middelkoop, Marcel van der Perk, Rens van Beek

Department of Physical Geography, Utrecht University, Heidelberglaan 2, 3584 CS, Utrecht, The Netherlands

ARTICLE INFO

Keywords:
Nitrogen
Phosphorus
Nutrient fluxes
Catchment models
Geographical information systems
Global change

SUMMARY

Nutrient discharge to coastal waters from rivers draining populated areas can cause vast algal blooms. Changing conditions in the drainage basin, like land use change, or climate induced changes in hydrology, may alter riverine nitrogen (N) and phosphorus (P) fluxes and further increase the pressure on coastal water quality. Several large scale models have been employed to quantify riverine nutrient fluxes on a yearly to decadal timescale. Seasonal variation of these fluxes, governed by internal nutrient transformations and attenuation, is often larger than the inter-annual variation and may contain crucial information on nutrient transfer through river basins and should therefore not be overlooked. In the last decade the increasing availability of global datasets at fine resolutions has enabled the modelling of multiple basins using a coherent dataset. Furthermore, the use of global datasets will aid to global change impact assessment.

We developed a new model, RiNUX, to adequately simulate present and future river nutrient loads in large river basins. The RiNUX model captures the intra-annual variation at the basin scale in order to provide more accurate estimates of future nutrient loads in response to global change. With an incorporated dynamic sediment flux model, the particulate nutrient loads can be assessed.

It is concluded that the RiNUX model provides a powerful, spatial and temporal explicit tool to estimate intra-annual variations in riverine nutrient loads in large river basins. The model was calibrated using the detailed RHIN dataset and its overall efficiency was tested using a coarser dataset GLOB for the Rhine basin. Using the RHIN dataset seasonal variable nutrient load at the river outlet can be satisfactorily modelled for both total N ($E = 0.50$) and total P ($E = 0.47$). The largest prediction errors occur in estimating high TN loads. When using the GLOB dataset, the model efficiency is lower for TN ($E = 0.12$), due to overestimated nutrient emissions. For TP, the model efficiency is only slightly lower ($E = 0.36$) in comparison to the RHIN dataset.

Despite the lower model efficiencies for the GLOB dataset, we conclude that this dataset provided reasonably good estimates of seasonal nutrient loads in the Rhine basin and is considered promising for application to other, less documented, large river basins.

© 2009 Elsevier B.V. All rights reserved.

Introduction

Large rivers are major suppliers of N and P to estuaries and coastal waters. Estimates of present riverine nutrient input to estuaries amount to 35.45–63.8 Mt N y^{-1} and 22 Mt P y^{-1} (Global) and 9.35–12.8 Mt N y^{-1} and 2.17–2.51 Mt P y^{-1} (North Atlantic) (Tappin, 2002). By regulating primary productivity, nutrient input from major rivers may affect the global carbon cycle on the long term. Because biological production consumes CO_2, and the carbon is (partly) sequestrated in burial of marine sediments over time, a close link between nutrient supply, primary productivity and climate change exists. On a shorter timescale, elevated nutrient concentrations may affect water quality by stimulating algal blooms to such extents that eutrophic waters show oxygen depletion and related fish mortality. This phenomenon is not only a local scale problem restricted to rivers and lakes in industrialised or intensive agricultural areas, but is already seen to affect large areas of adjacent coastal waters (Rabalais et al., 2002) on which vast population numbers depend their living. With growing population the pressure on the coastal waters is likely to further increase in the future. Improved wastewater treatment, on the other hand, may reduce per capita nutrient loads. Global change can also alter nutrient fluxes by causing a shift in the hydrological balance of the river basin. Higher runoff can potentially increase the mobility of nutrients (temporarily) stored in the river basin. Even when mean runoff may not change on the long term, seasonal changes (e.g. higher winter runoff in combination with lower summer runoff) may alter

* Corresponding author. Tel.: +31 30 2532754; fax: +31 30 2531145.
E-mail address: s.loos@geo.uu.nl (S. Loos).

0022-1694/$ - see front matter © 2009 Elsevier B.V. All rights reserved.
doi:10.1016/j.jhydrol.2009.02.019

the mobility of nutrients. Therefore, not only spatial variation, but also short-term (seasonal) temporal variability is of importance when considering future riverine nutrient transport to coastal waters. The importance of the ratio in which nutrients are supplied to coastal waters, requires the combined modelling of both N and P loads. Thus global change impacts (emission and climate) assessment require a seasonal, distributed model for both N and P that is easily transferable between large river basins.

In recent years many modelling studies (Caraco and Cole, 1999; Van Drecht et al., 2003; Seitzinger et al., 2005; Wollheim et al., 2008) have made considerable progress in estimating nutrient fluxes at the land–ocean transition. The key processes of the N and P cycles are included in most nutrient export models. However, different process descriptions (empirical, conceptual, or process-based) are used. Large scale models often use a lumped or semi-distributed representation of the river basin (Caraco and Cole, 1999; Seitzinger et al., 2005). Spatial simplifications may be appropriate for static modelling of present conditions, but is likely to be inadequate for future predictions where spatial variability in nutrient stock related to landscape properties (relief, soil type, land use, population density) may respond differently to external forces (precipitation, temperature, runoff). Furthermore, most large scale models do not account for the basic physics that drive the seasonal variation (e.g. yearly temperature cycle, monthly precipitation trend, fertilizer application during growing season). The contribution of particulate bound nutrients is often not explicitly modelled in large scale nutrient export models. Some models (Caraco and Cole, 1999; Beusen et al., 2005) estimate particulate nutrient load based on an empirical relationship; distributed suspended sediment transport for nutrient transfer, however, has not yet been incorporated. Basin to small scale models on the other hand, such as Riverstrahler (Billen et al., 1994), which incorporate intra-annual variation, are often too complex and unsuitable for large scale modelling. Insufficient data availability and computational time restriction hamper the use of these detailed nutrient models.

There is a lack of models designed for the intermediate, large basin scale. A few models designed for the catchment scale (from 1 km^2 to >1000,000 km^2) exist, like the HBV-NP (Arheimer and Brandt, 1998; Andersson et al., 2005) and PolFlow (De Wit, 2001). The HBV-NP model, however, use field-scale sub-models that are highly data demanding. The PolFlow model was designed to model average N and P loads for 5-year periods and is therefore inappropriate for seasonal timescale modelling. It has been applied to several larger catchments (e.g. Rhine, Elbe, Po).

The different approaches and the large variation in model results show that it remains difficult to simulate the key processes properly. So far, most difficulties exist in simulating riverine phosphorus fluxes (Johnes, 2007) partly due to the complex interaction with suspended sediments. Uncertainties in nutrient emission (e.g. animal excretion rates, crop uptake), especially at the regional to global scale, further frustrate nutrient modelling and contribute to different model results.

With the increasing availability of global scale datasets at fine resolutions (Table 3), allocation of nutrient input has improved since the beginning of the 1990s. Good allocation is essential as it affects the distance and time nutrients are subject to within-stream attenuation. This enables us to fill the gap between detailed but data-demanding models designed for individual river basins and coarse scale models, both in space and time, designed for global applications. Global scale datasets have already proven successful in dynamic hydrological models (Alcamo et al., 2003) and sediment flux models (Syvitski et al., 2005). Now progress can be made in the dynamic modelling of nutrients.

The aim of this study was to assess nutrient fluxes at the larger basin scale using global datasets. For this purpose, (1) a dataset (GLOB) was assembled from globally available data sources, and (2) a new model RiNUX was developed to calculate riverine nutrient loads at the large river basin scale using these globally available data. This model is based on existing concepts and accounts for the sources and the seasonal and long-term variability of both dissolved (DN, DP) and particulate (PN, PP) transport of nitrogen and phosphorus. We tested the applicability of the GLOB dataset in the RiNUX model for the well-documented Rhine river basin (Kwadijk and Middelkoop, 1994; De Wit, 1999; Behrendt et al., 2000; Asselman et al., 2003). To this end, we calibrated the RiNUX model against observed river nutrient data using a second more detailed input dataset (RHIN) assembled by De Wit (1999). It was assumed that this 1 km × 1 km resolution dataset, adequately represents the spatial and temporal variability of nutrient inputs within the Rhine basin. Subsequently, we applied the calibrated model using the coarser-resolution GLOB dataset and evaluated the model results using observed riverine nutrient fluxes in the Rhine river.

In this paper the model structure and performance for present-day conditions are presented. Eventually, RiNUX aims to adequately simulate future N and P loads in large river basins for global change impact assessment.

Rhine river basin

The river Rhine is the largest river draining into the North Sea and has an upstream area of 185,000 km^2 (160,000 km^2 upstream from Lobith (Fig. 1) at the Dutch–German border). The mean discharge is 2300 $m^3 s^{-1}$ at Lobith (Middelkoop and Van Haselen, 1999). The Rhine is highly impacted by human activities: The

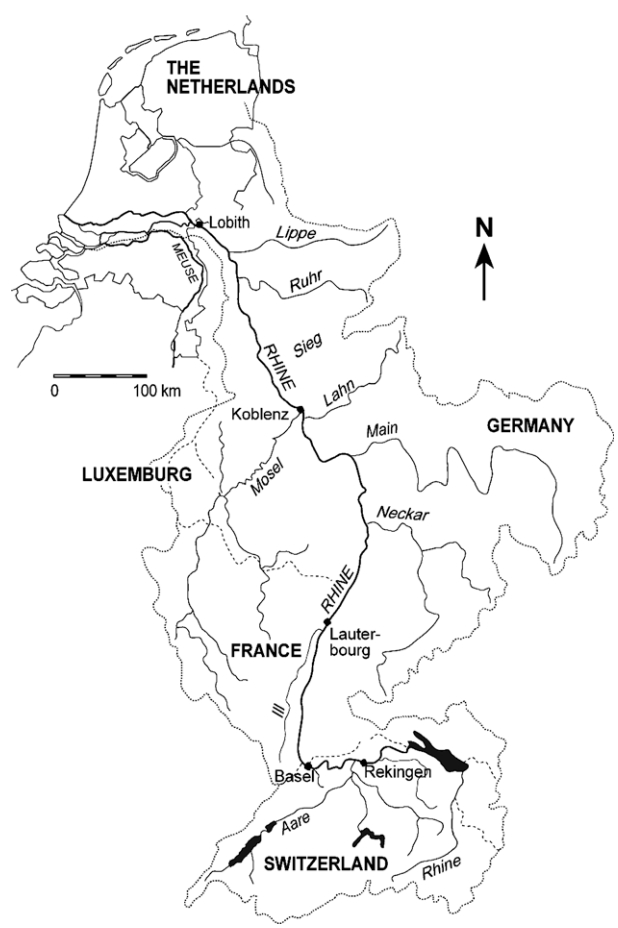

Fig. 1. Tributaries and monitoring stations in the Rhine Basin.

Rhine river basin is occupied by 58 million inhabitants (46 million upstream of Dutch–German border) and the mean population density of around 300 people km^{-2} is among the highest in the world. Besides urbanisation, agriculture puts a major pressure on the coastal environment through the application of large amounts of industrial fertilizers (Crossland et al., 2005). Agricultural area covers the largest part of the Rhine basin (about 50%), followed by forest (over 35%), and built-up area (about 8%). Just over 1% of the basin is covered by in-land waters. Although this is only a minor fraction, these lakes trap large amounts of sediments and associated nutrients (Syvitski et al., 2003).

The nitrate concentration (minimum: 0.86 mg N l^{-1}, maximum: 6.56 mg N l^{-1}; IKSR, 2004) of the Rhine at Lobith (Dutch–German border), observed between 1970 and 2003 contributes 86.9% to the mean total N (TN) concentration. The average nitrate concentration is 18 times higher than the global maximum (0.2 mg/l; Meybeck, 1993) in unpolluted major rivers. For the downstream reaches Venterink et al. (2003) reported PN concentrations up to 0.14 mg N l^{-1}. These fractions, however, do not contribute much to the TN load in the Rhine. At Lobith, the average observed TN load ranged between 2174 and 2938 kg N km^{-2} y^{-1} in the period from 1970 to 1995. The concentration of phosphate in the Rhine at Lobith over the same period has an average of 0.19 mg P l^{-1} (IKSR, 2004). This lies well above median pristine (0.010 mg P l^{-1}; Meybeck, 1993) and world median concentrations (0.025 mg P l^{-1}; Global GEMS in Meybeck, 1993). Phosphate forms 33.8% of the median total P (TP) concentration in the Rhine; the largest part is transported downstream as particulate phosphorus (PP). During a short measurement campaign in downstream parts of the river PP and DOP were found to be the major P fractions (Venterink et al., 2003). Observed TP loads at Lobith decreased from 363 kg P km^{-2} y^{-1} to 77 kg P km^{-2} y^{-1} in the period from 1970 to 1995. The suspended sediment load in the river Rhine at Rees station (Dutch–German border) is about 3.14×10^6 t y^{-1} (Asselman, 2000) of which the tributaries Aare, Main, Neckar, and Mosel rivers are the largest suppliers (Asselman et al., 2003). Nitrogen content from 11 suspended sediment samples taken from the middle Rhine (at Lauterbourg) between January 1996 and June 1997 averaged 0.5 wt% (Lartiges et al., 2001). Suspended sediment samples taken between 1989 and 2007 at Lobith showed a total P content of 0.05–1.3 wt% with an average of 0.21 wt% (Waterbase, 2008).

Both nitrogen and phosphorus loads in the Rhine show strong seasonal fluctuations (Fig. 2). The nitrogen loads are highest during winter, when the water discharge is large and the TN concentrations are high. During warmer months, the discharge is relatively low and enhanced nutrient uptake in the watershed (Ahad et al., 2006) is a likely cause for the observed low TN concentrations in summer. For phosphorus a similar trend is visible, although less pronounced.

Different nutrient transport models have been applied to the Rhine Basin varying from empirical (Caraco and Cole, 1999; Seitzinger et al., 2002, 2005) to more process-based (Behrendt, 1996; De Wit, 2001; Van Drecht et al., 2003), with different spatial resolution (0.5 arc deg to 1 km). The PolFlow model (De Wit, 2001) is a distributed model and calculates the average nutrient loads at a 5-year temporal resolution. PolFlow was initially developed for the Rhine Basin using an extensive dataset for the period 1970–1995. It performs quite well with an average relative error of 13%.

Behrendt et al. (2000) used the conceptual, static, semi-distributed MONERIS model to calculate the nitrogen load in the river Rhine and estimated 2472 kg N km^{-2} y^{-1} for the period 1983–1987, and 1736 kg N km^{-2} y^{-1} for the period 1993–1997, resulting in a deviation between calculated and observed loads of less than 30%. Van Drecht et al. (2003) estimated a yearly mean of 2865 kg N km^{-2} y^{-1} (*observed*: 2448 kg N km^{-2} y^{-1}) exported at the mouth of the Rhine using a global static model. The empirical lumped model by Caraco and Cole (1999) estimates the nitrate export to be just less than 1200 kg NO_3–*N* km^{-2} y^{-1} (*observed*: 1520 kg NO_3–*N* km^{-2} y^{-1}). Both models have not been calibrated for individual rivers, but were used for estimating globally distributed N export from large river basins.

Model concepts and methods

Model overview

The RiNUX model simulates N and P transport in large river basins at 1 km × 1 km grid and monthly resolution. It consists of three sub-modules: a soil module, a groundwater module and a surface water module (Fig. 3). The model has been implemented in the PCRaster environmental modelling language (Wesseling et al., 1996). The nutrient surplus at the land-surface calculated for each grid cell is stored in the soil compartment or transported, directly or via the groundwater compartment, to the surface water (river/lake) in which it is routed towards the river outlet. Water and sediment fluxes, the main agents for dissolved and particulate nutrient transport, govern the transport of nutrients between the compartments. The water fluxes (surface runoff, percolation, groundwater discharge, and river discharge) are calculated with an adapted version of the global hydrologic PCRglobWB model (Van Beek and Bierkens, 2006), which is a water balance model based on the HBV concept (Bergström, 1995; Fig. 4). Sediment fluxes (sediment delivery to the channel) are calculated in a soil erosion model based on the RMMF model (Morgan, 2001), which was redesigned for application to large river basins.

Hydrology

The hydrological model accounts for water storage in an interception store, a snow cover, and two soil stores (Fig. 4). Before precipitation reaches the upper soil store ($PREC_{eff}$; m day^{-1}), part of the intercepted water in the canopy store is lost through evapora-

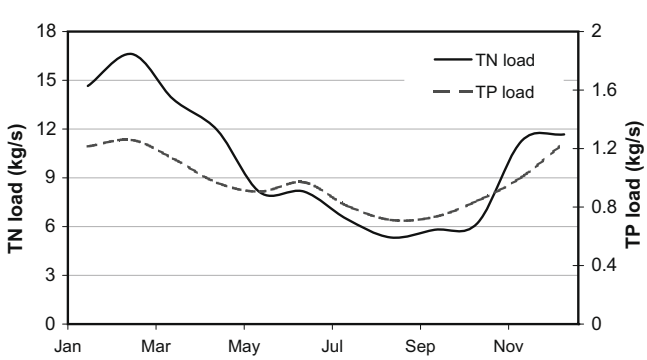

Fig. 2. Monthly averaged N and P loads for the monitoring station at Lobith.

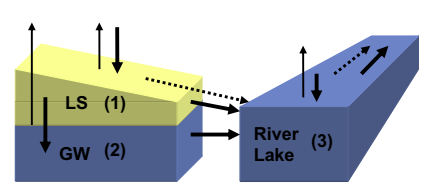

Fig. 3. RiNUX flow diagram. Nutrients are transferred between three landscape compartments: (1) the soil (LS), (2) groundwater (GW) and (3) surface waters (River/Lake). Two independently run models (hydrological and erosion model) provide water and sediment fluxes that drive the transfer of nutrients. The nutrient transfers between the different compartments are highlighted with the thick (dissolved) and dashed (particulate) arrows. In each 'store' losses may occur (thin arrows).

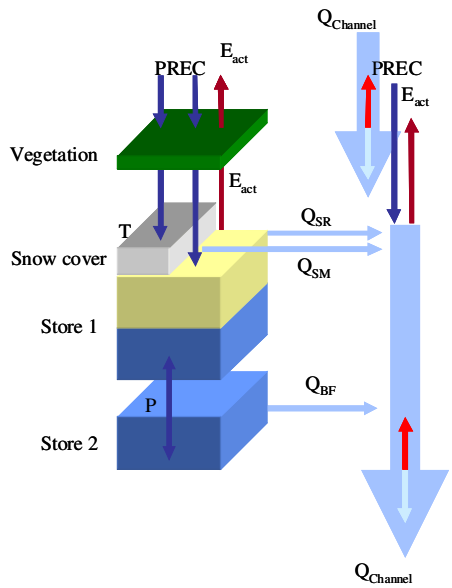

Fig. 4. Flow scheme of the hydrological model.

tion. The upper groundwater store ($St1$) has a limited storage capacity ($Stc1$; m), whereas the lower store ($St2$; m) has an 'infinite' volume. The quick runoff (Q_{QR}; m day^{-1}) is dependent on the degree of saturation of the upper store:

$$Q_{QR} = \left(\frac{St1}{Stc1}\right)^{\beta 1} \cdot (PREC_{eff} + SC_{melt}) \tag{1}$$

where SC_{melt} is snow melt (m day^{-1}) and $\beta 1$ is the shape coefficient of direct runoff (–), which is a function of slope and degree of saturation at field capacity. The water stored in the upper store can never exceed its storage capacity, but spills the excess water to the quick runoff. Quick runoff is defined as rainfall surface runoff (Q_{SR}) plus snowmelt surface runoff (Q_{SM}). Snowmelt is calculated based on thickness of the snow cover (SC (m)) and a degree-day melt factor (m °C^{-1} day^{-1}). From the upper store water can percolate (P; m day^{-1}) to the lower groundwater store based on the saturated conductivity ($ks1$; m day^{-1}) and the relative soil moisture content of the upper soil store (Eq. (2)).

$$P = \min\left(St1 + PREC_{eff} - Q_{QR}, ks1 \cdot \left(\frac{St1}{Stc1}\right)^{\beta 2}\right) \tag{2}$$

where $\beta 2$ is the shape coefficient relating the unsaturated hydrologic conductivity to the degree of saturation (–). Baseflow (Q_{BF}; m day^{-1}) is calculated using a first order recession constant. In accordance with the scheme in Fig. 4, the daily water balance is calculated for each grid cell. The model is fed by daily climate data (precipitation ($PREC$), evaporation (E_{act}) and mean temperature (T)) obtained from the ERA-40 Re-analysis dataset (Uppala et al., 2005). The river discharge ($Q_{Channel}$; m^3 day^{-1}) is calculated from the sum of surface runoff and baseflow which is routed downstream along a local drainage direction (LDD) grid. Lakes are treated differently; it drains water when water height (WH_{lake}; m) exceeds a fixed spill-level (WH_{outlet}; m):

$$Q_{lake} = \lambda \cdot (WH_{lake} - WH_{outlet})^{1.5} \tag{3}$$

where λ is a calibrated discharge coefficient (m^2 day^{-1}). For the nutrient model, the daily water fluxes are aggregated to monthly values.

Sediment yield and transport

The sediment yield submodel is based on the RMMF model. The sediment yield submodel considers soil detachment by raindrop impact (rain splash) (F), detachment by overland flow (H) and hillslope sediment transport by overland flow. As the RMMF model is intended for plot scale use, an adjustment to the transport capacity (TC) concept was made for large scale application. The basic process formulations, however, remained largely unchanged.

The same precipitation data that forces the hydrological submodel was used for the sediment yield submodel. Overland flow was calculated according to RMMF. Note that this overland flow is smaller than the quick runoff as calculated by the hydrological submodel (Eq. (1)) as the latter also includes snow melt and near-surface runoff. To apply the original RMMF model to large scale basins, initially the basin was divided into small sub-catchments at a 90 m resolution, using the SRTM digital elevation data (CGIAR-CSI, 2004). Each sub-catchment was further divided into a riparian part (the grid cell bordering the river channel) and an upstream part (the remaining grid cells). For the calculation of H and TC, the overland flow was scaled using a scaling parameter representing the number of concentrated rills per grid cell width. For each sub-catchment, the amount of sediment entering the river network equals F plus H in the sub-catchment, maximised by the TC in the riparian grid cell. The RiNUX model used this sediment delivery flux in combination with soil nutrient content to calculate the particulate nutrient input from hillslopes. This sediment supply from the hillslope (SD; kg mth^{-1}) was added to the river sediment store (St_{chan}; kg).

The sediment transport in the river channel was calculated using:

$$Y_{chan} = \varepsilon \cdot Q^2 \cdot S_{chan} \tag{4}$$

where Y_{chan} is the sediment transport (kg mth^{-1}), ε is an erosion constant (kg s m^{-3} mth^{-1}), Q is discharge (m^3 s^{-1}) and S_{chan} is the channel bed slope (–). For low discharges an erosion threshold ($Y_{threshold}$; kg mth^{-1}) was introduced. Below this threshold, the resuspension of sediment from St_{chan} into transport was zero and the river was assumed to transport a minimum suspended sediment load (washload that stays in suspension at low discharges; S_{wl} (kg mth^{-1})) in accordance with a study by Doomen et al. (2008). Once the sediment is in suspension the material is transported all the way down to the river outlet even if in downstream cells the erosion threshold is not met. The sediment delivery to the downstream channel cell is thus the washload added to the suspended sediment load from its upstream cell (excluding washload) plus an optional supply from the river sediment store.

In lakes only a fraction of the sediment delivered from upstream channels was transported downstream. This fraction linearly depends on the lake residence time.

Nutrient fluxes

The soil module (Fig. 5; (1) in Fig. 3) is the 'core' of the RiNUX model; here the net input of nutrients from diffuse sources is added to the soil store, which consists of a labile and stable pool. The nutrient balance per grid cell is calculated by adding up the input amounts (inorganic fertilizers, manure excretion by livestock, atmosphere deposition (N), biological N fixation and weathering (P)) minus direct losses (via volatilization and nutrient loss in crop yield). Subsequently, the surplus is transferred to either the GW store (via leaching) or directly to the surface waters (via surface runoff; in dissolved or particulate form), lost to the atmosphere (via denitrification (N)), or (temporarily) stored in the soil. The pathways of the nutrient surplus are primarily influenced by the

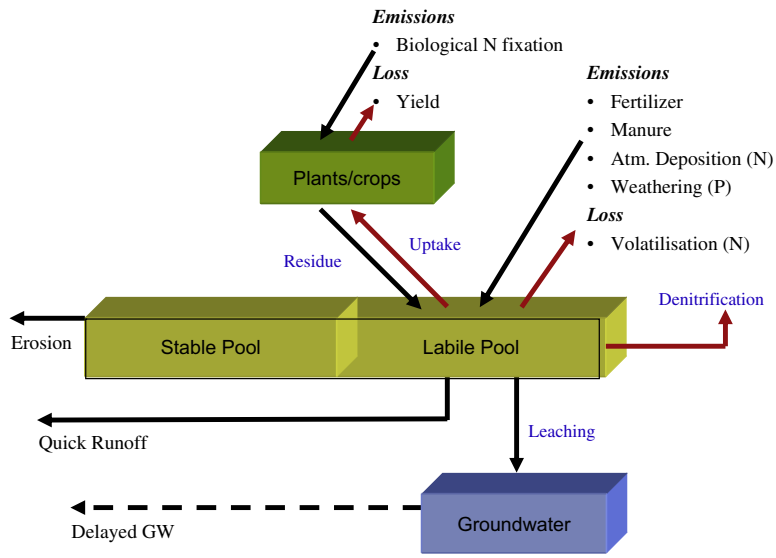

Fig. 5. The soil module calculates the land-surface nutrient balance and considers inputs from fertilizer and manure application, atmospheric deposition (N), biological N fixation, weathering (P) and 'losses' via volatilization (N), yield, erosion, denitrification, and leaching.

hydrological fluxes, but also by soil properties, nutrient availability, and climatic factors such as temperature.

Soil nutrient inputs

The calculated monthly nutrient surplus is added to the labile pool, as its mobility is high at the time of emission. Inputs from fertilizer, and manure and N fixation by legume crops follow a seasonal trend in line with crop and plant requirements and were added to the labile soil pool at the start of the growing season. The N input from natural N fixation was distributed equally over the 12 months. The input from atmospheric N deposition was spread equally over the months each year and added as a diffuse source to the soil store or added directly to surface water in lakes. Phosphorus contribution from bedrock weathering was calculated by multiplying a mean rock weathering rate, 27.5 t km^{-2} y^{-1} (Newman, 1995), with mean P concentration per rock type as in Table 1 and was added to the labile pool.

Emission from population not connected to sewers is assumed to be a diffuse source and was therefore added to the labile soil pool. Nutrients from sewage systems were added directly to surface waters.

Soil nutrient losses

Soil nutrient losses include losses through harvest, losses via surface runoff and leaching to groundwater, denitrification, and volatilization. The latter two processes only apply to N. Nutrient loss by crop harvest was accounted for by incorporating a yield term which was removed equally throughout the growing period of the crops, simulating the uptake by plants.

Loss of particulate nutrients (PN; kg mth^{-1}) to surface water via surface runoff was calculated by multiplying the monthly sediment yield (SD; kg mth^{-1}), calculated in the soil erosion model, by the dynamic fractional soil nutrient content (N_{tot}; kg kg^{-1}) of the topsoil layer (20 cm) and removed from the soil stable pool:

$$PN = f_{stable} \cdot N_{tot} \cdot SD. \quad (5)$$

where f_{stable} is the stable fraction (–). The dissolved part transported in surface runoff (DN; kg mth^{-1}) is calculated under the assumption that the labile nutrient pool is spread equally in the top meter of the soil column for N and in the top 10 cm for P as P is more concentrated in the upper soil layer (Owens and Deeks, 2004). The concentration in the soil is calculated by dividing the labile pool by the soil water store. This concentration is multiplied by the amount of surface runoff to obtain the quick component of the nutrient load that enters the surface water.

Denitrification in the soil is modelled using the concept of Van Drecht et al. (2003) in which various factors influence the denitrification rate, namely soil texture, drainage conditions and soil organic carbon content, and temperature and residence time in the rootzone. Residence time in the rootzone ($RT_{rootzone}$; y) is estimated by dividing the storage capacity of the topsoil up to 1 m below the surface ($Stc1$; m) by the annual precipitation (P_{yr}; m y^{-1}):

$$RT_{rootzone} = Stc1/P_{yr} \quad (6)$$

Denitrification is assumed to be inhibited if air temperature is below 0 °C.

After all losses are removed from the labile pool, the remaining nutrients in the labile pool can leach to the deeper groundwater. The leaching rate is assumed to be proportional to the water percolation rate ($Perc$; m mth^{-1}) and the 'saturation' state of the labile pool (N_{lab}/NM_{lab}). In case the actual N content (N_{lab}) exceeds a maximum labile pool capacity (NM_{lab}), due to newly added nutrient from the various inputs, the maximum of the nutrient excess and the calculated leachate amount is taken, assuming a saturated labile pool. To prevent unrealistic high N concentrations in the percolating water when the water flux is very small, the concentration is maximised to 400 mg l^{-1}.

Groundwater

The groundwater functions as a reservoir that is fed by monthly leachate loads in which delay and retention takes place before the resulting nutrient load is discharged to the surface water. From the input, the leaching concentration (C_{in}; mg l^{-1}) and groundwater

Table 1
P concentrations (mg g^{-1}) in rock types (Newman (1995)).

Rock type	Mean phosphorus concentrations (mg g^{-1})
Continental crust, surficial rock	0.6–1.2
Igneous rocks	0.6–1.3
Sedimentary rocks	
Shales	0.7
Sandstones	0.4
Carbonates	0.2

recharge (Q_{in}; mm y^{-1}), to the aquifer, the groundwater concentration (C_{gw}; mg l^{-1}) can be calculated as follows:

$$C_{gw} = \frac{C_{gw,prev} \cdot \tau \cdot Q_{out,prev} + C_{in} \cdot Q_{in}}{Q_{out} \cdot (1+\tau)} \quad (7)$$

where τ is the mean residence time (y) for a given area that water stays in the groundwater store before exfiltration to the surface water. As Eq. (7) applies to steady state conditions the long-term average recharge (mm y^{-1}) was used for Q_{in}. The groundwater flux, Q_{out}, was calculated as follows:

$$Q_{out} = f \cdot Q_{out,prev} + (1-f) \cdot Q_{in} \quad \text{with} \quad f = \frac{\tau - 0.5 \cdot \Delta T}{\tau + 0.5 \cdot \Delta T} \quad (8)$$

where ΔT is the model time step (y) and f determines the strength of the 'memory' effect of the groundwater concentration based on the residence time. τ is calculated differently for lowland and upland aquifers. For lowland areas, τ is estimated using:

$$\tau = \frac{nD}{N} \quad (9)$$

where n is aquifer porosity (–), D is saturated aquifer thickness (m), and N is aquifer recharge rate (m y^{-1}). As no adequate aquifer thickness is available, a value of 50 m was chosen for the whole basin, independent of the aquifer type, in accordance to the approach of De Wit (1999). For consolidated rocks in upland areas, the groundwater residence time was calculated according to McGuire et al. (2005):

$$\tau = 0.0021 \cdot \frac{L}{G} + 0.71 \quad \text{and} \quad L = 0.5 \cdot \frac{1}{DD} \quad (10)$$

where L is flow path length (m), G is flow path gradient (–), and DD is drainage density (m m^{-2}).

The groundwater module was run with a time step (ΔT) of one year, as the groundwater nutrient concentration is assumed not to show any seasonal variation, given that the majority of the groundwater residence time >1 y. Part of the groundwater nutrient flux is lost through denitrification (N) or adsorption (P) during transport. The fraction retained in the groundwater reservoir is estimated by assuming that the chance of groundwater flowing through a retention zone, in which all nutrients are denitrified, increases with age. Accordingly, the actual nutrient load transport from groundwater to surface water (L_{gw}; kg mth^{-1}) was calculated using:

$$L_{gw} = C_{gw} \cdot 1000 \cdot Q_{BF} \cdot 0.5^{(\tau/\tau_{zero})} \quad (11)$$

where τ_{zero} (y) is the travel time at which half of the leached nutrients are retained and Q_{BF} is the baseflow as calculated in the hydrological model.

Within-channel processes

Within-channel nutrient attenuation was modelled using two retention parameters α_1 and α_2:\

$$\alpha_1 = D_{rate} \cdot \max(0, T_{mth} - T_{crit})^{Pt} \quad (12a)$$

$$\alpha_2 = \frac{1}{1 + (Psw_1 \cdot (100 \cdot S + 1)) \cdot (Q+1)^{Psw_2}} \quad (12b)$$

where D_{rate} is the denitrification rate constant (°C^{-1}), T_{crit} is the critical temperature under which denitrification is inhibited (°C), Pt is a parameter describing the temperature attenuation relationship (–), and Psw_1 and Psw_2 are parameters describing overall loss and relative headwater loss, respectively (–). α_1 (–) represents the attenuation fraction as a result of biological uptake for which temperature is taken as a proxy. α_2 (–) originated from the PolFlow model (De Wit, 2001) and represents the fraction retained caused by loss to floodplains (slope (S) is used here as a proxy for their occurrence) or long in-stream residence times (where discharge, Q, is a proxy for the residence time in the channel). By combining the two parameters into one transfer function (α_{river}), the fraction that is transported to the downstream cell is calculated as:

$$\alpha_{river} = 1 - \frac{\alpha_1 + \alpha_2}{2} \quad (12c)$$

The attenuation as a result of biological uptake (α_1) was also applied to particulate associated nutrients. Retention of particulate nutrients due to sedimentation and retention in lakes and reservoirs was simulated as the retention of sediment described in "Sediment yield and transport". The attenuation of dissolved nutrients in lake and reservoir systems was linearly related to water residence time.

Model initialization and calibration

For the initial state of the stable pool the soil nutrient content from the FAO soil database (Batjes, 1996) was taken for the top 100 cm, the maximum depth that is assumed to contribute to removal of dissolved nutrients by quick runoff. The labile pool content was initially set to zero, assuming all labile fractions have been washed out the topsoil prior to new nutrient loading. A fixed long-term transfer of 25 kg ha^{-1} from the labile to non-labile pool was assumed for agricultural soils. Mineralization of organic (non-labile) nutrient fractions to inorganic nutrient fractions was not included in the current RiNUX version.

The groundwater concentration was initialized by a 20 year run from 1950 to 1970 using a linear increase in loading from zero in 1949 to the nutrient surplus in 1970.

Monthly averaged discharge at Lobith was used for calibrating the hydrological model. The years 1970–1980 were used as spin-up for the model. $Y_{threshold}$ and ε were calibrated by fitting the mean annual suspended sediment flux at Lobith over the period 1984–2000 against the observed mean for the same period. S_{wl} was taken by taking the minimum observed concentration at the outlet station. The nutrient parameters were calibrated with trial and error, taking in to account the ranges for p and τ_{zero} (Table 2).

Data for model input and validation

The various GIS layer maps used in all modules of the RiNUX model are listed in Table 3. First, the RiNUX model was run and calibrated with the best available emission dataset, RHIN, of De Wit (1999) against TN and TP loads at Lobith. Subsequently, the calibrated model was run with the global GLOB emission dataset (Table 3) to test the model performance using this coarser dataset at the large river basin scale as input. The RHIN and GLOB datasets contained the same hydrological and sediment input data. However, most nutrient input and loss maps differed between the datasets.

The hydrological model was run using climate data from the ECMWF 40 Year Re-analysis (ERA-40) Data Archive (precipitation, temperature, evaporation). The ERA-40 global dataset consists of daily maps covering the period from mid-1957 to mid-2002. Hydrological data (daily discharge) was obtained from the GRDC (2007) for 18 stations and daily suspended sediment load measurements were obtained from BfG (2007). Water quality data TN and TP loads (measured twice a month) was obtained from IKSR (2004).

The RHIN dataset contains diffuse emission maps (fertilizer and manure application, crop nutrient yield, atmospheric deposition, and household wastes from population not connected to sewerage) and point source emission maps (separate maps for emission from sewage and waste water treatment plants (WWTPs), and from industries) for five succeeding periods of 5 years starting from 1970, that was assembled on a sub-national to district level (in total 415 areas) for the entire Rhine

Table 2
Parameter description.

Parameter	Description	Method of estimation	Value
Hydrology			
$\beta 1$	Shape coefficient for direct runoff (–)	Scaled to the area with deep groundwater and available soil moisture storage at field capacity	Distributed
$\beta 2$	Shape coefficient relating the unsaturated hydrologic conductivity to the degree of saturation (–)	Log-linear relationship between unsaturated hydrologic conductivity and degree of saturation of the upper store	Distributed
Λ	Discharge coefficient (m^2 s)	Calibrated against discharge data	0.34
Sediment			
ε	Channel bed erosion constant (kg s m^{-3} mth^{-1})	Best guess estimate	1.5
$Y_{threshold}$	Threshold above which erosion from river store takes place (kg mth^{-1})	Best guess estimate	0.0375
S_{wl}	Minimum suspended sediment load (washload) (kg mth^{-1})	Based on the minimum observed concentration at the basin outlet	Distributed
Nutrients			
NM_{lab}	Maximum labile pool capacity (kg m^{-1} depth)	Soil nutrient content in 1945 · parameter value	0.01 (N) 0.013 (P)
τ_{zero}	Groundwater travel time at which half of the leached nutrients are retained (y)	A priori range 1–100 y	60 (N) 10 (P)
Pt	Parameter describing the temperature attenuation relationship (–)	A priori range 1–3	2.2 (N) 1.15 (P)
Psw_1	Parameter describing overall loss within stream (–)	Best guess estimate	50 (N) 50 (P)
Psw_2	Parameter describing relative headwater loss (–)	Best guess estimate	3 (N) 3 (P)
D_{rate}	Surface water attenuation rate (°C^{-1})	Best guess estimate	0.000009 (N) 0.0001 (P)

Table 3
Overview of data used as input to the various modules: hydrology, sediment and nutrients (GLOB dataset).

Input variable	Year	Resolution	Source	Application
General				
Digital elevation model	–	1 × 1 km	GTOPO30/HYDRO1k (1996)	Routing of water, sediment, and nutrients
Land cover	1992/1993[a]	30 s	IFPRI (2002)	Allocation of agricultural area, populated areas, and lakes
Percent tree cover	2002	30 s	De Fries et al. (1999)	Allocation of forested area
Soil properties (soil texture, drainage conditions, organic carbon content)	–	5 min	FAO-UNESCO (1995)	Various applications
Hydrology				
Daily temperature, precipitation, actual evaporation	1970–2002	125 × 125 km	ERA-40, Uppala et al. (2005)	Climate input
Sediment				
SRTM	–	90 m	CGIAR-CSI (2004)	Slope
Nutrients				
Soil N content (0–20 cm/20–100 cm)	–	5 min	FAO-UNESCO (1995)	Relative nutrient content in soil layers
Lithology map	–	Polygons	Dürr et al. (2005)	Diffuse emission input
NO_y/NH_x deposition (EU and US)	1978–1994[b] 1989–1994[c]	0.5°	EMEP[d]/NADP[e] (Holland et al., 2004)	Diffuse emission input
NO_y/NH_x deposition (global)	1993	3.75° × 5°	Dentener (2006)	Diffuse emission input
Fertilizer application	1993	5 min	FAOSTAT (2006) + Leff et al. (2004) + FAO (2002)	Diffuse emission input
Manure application	2000	3 min	FAO (2007) (GLiPHA[f]) + excretion rates	Diffuse emission input
NH_3-loss	1993	5 min	Bouwman et al. (2002)	Diffuse emission loss
Yield (crop harvest)	1993	5 min	FAOSTAT (2006) + Leff et al. (2004) + Bouwman et al. (2005)	Diffuse emission loss
Global population	2002 1990–2015	30 s 2.5 min	LandScan (2002) CIESIN (2005)	Point emission input

[a] The PAGE Agric. Extent update (version2) was performed based on an improved interpretation of the 1992/93 AVHRR that was released in 2000. The land use–land cover map is adapted from this interpretation.
[b] Wet deposition.
[c] Dry deposition.
[d] EMEP (Convention on Long-range Transboundary Air Pollution (Europe)).
[e] NADP (National Atmospheric Deposition Program (US)).
[f] Global Livestock Production and Health Atlas.

basin. The GLOB dataset with global coverage was assembled for this study, into various GIS layers of various resolutions (Table 3). This dataset contains emission maps for the same nutrient sources or losses as in the RHIN dataset, except that no distinction is made between point source emission from households and industries. Additionally, the GLOB dataset contains N emis-

sion maps of biological N fixation, NH_3 loss (volatilization), and a map of P emission from rock weathering. These emission maps were also used to complete the RHIN dataset. Although some of the emission maps may link back to identical data sources (e.g. trends in crop yield amounts and fertilizer consumption (FAOSTAT, 2006)), differences exist in all input maps due to differences in the applied scaling and aggregation techniques or differences in the crop- or excretion coefficients used. All maps in the RHIN dataset are based on data for 415 administrative units, whereas the GLOB dataset is based largely on data at the country level or other coarse resolutions as listed in Table 3.

From the FAOSTAT dataset, national trends in fertilizer loading, livestock numbers and crop yield statistics were obtained. The distribution of the applied fertilizer over cropland and grasslands was calculated using crop area and crop specific fertilization rate (country based relative fertilization rates per crop (FAO, 2002)) if available, or by using mean fertilization rate per agricultural area. Crop area was calculated from the crop distribution given by Leff et al. (2004) rescaled to meet FAO country statistics for the year 1992. Although yearly harvested area changes according to FAO statistics the crop distribution was fixed in time in the model. The GLiPHA sub-national livestock database (FAO, 2007) provided globally distributed maps of dominant livestock species and numbers for the year 2000. The livestock numbers were recalculated to 1993 values using the FAOSTAT dataset. The spatial distribution was assumed to have been constant in time. Manure production maps were derived by combining these maps with excretion rates as listed in Table 4. N fixation by crops was based on fixation rates of N-fixing crops (Table 5) in combination with FAO derived crop areas, whereas fixation by natural vegetation was modelled following Cleveland et al. (1999). Atmospheric deposition of NH_x–*N* and NO_y–*N* was estimated from mean long-term spatially differentiated values taken from Dentener (2006) and Holland et al. (2004) for the year 1993. Deposition in other years was estimated by assuming a linear trend between the year 1993 and the reconstructed emission in 1860 or the predicted deposition in 2050 reported by Dentener (2006). Volatilization losses were derived from a global dataset of Bouwman et al. (2002). This dataset was used for the year 1993. Volatilization loss for all other years was estimated by scaling the loss to the relative application of both fertilizer and manure in other years compared to that in 1993. Since manure is generally subject to higher volatilization rates than other fertilizers, NH_3 loss estimates were calculated according to Bouwman et al. (2002) to be 21% and 7%, from manure and fertilizer, respectively. Crop yield was calculated based on the crop areas, the annual crop yield statistics (FAOSTAT, 2006), and nutrient content per crop (Table 6).

N from point source emission was calculated using the dataset provided by Bouwman et al. (2005). An adjustment to their approach was made by including emission from the rural population in the same way as the urban population. For P from point source emission a similar approach was used by assuming a N:P ratio of 6 for total emission per inhabitant per year according to the values published by Kristensen et al. (2005). Furthermore, for WWTP's we assumed a slightly higher (1.28 times) removal efficiency for P than for N (based on data provided by Kristensen et al., 2005).

It is assumed that the land use, important for the allocation of nutrient inputs, only shows temporal changes at sub-basin level and that most of these changes are already implicitly taken into account by the population numbers and crop areas that are variable in time.

Table 4
Livestock excretion rate estimates.

	kg N head^{-1} y^{-1}	kg P head^{-1} y^{-1}
Bovine	50	9
Buffaloes	30	7
Cattle	70	11
Small ruminants	10	1.9
Goats	10	1.9
Sheep	10	1.9
Pigs	15	3.5
Poultry	0.6	0.2

Source: best guess from Smil (1999) and Schreiber et al. (2003).

Table 5
Biological N fixation rates (Schreiber et al., 2003).

Crop type	kg N ha^{-1} y^{-1}
Pulses	80
Clover	240
Alfalfa	240
Other legume crops	25
Free living organisms	
Permanent crops	5
Permanent pasture	5

Table 6
Crop yield nutrient content estimates (Bouwman et al., 2005).

Crop type	N content (kg N kg^{-1})	P content (kg P kg^{-1})
Barley	0.017	0.0036
Cassava	0.002	0.0004
Seed cotton	0.029	0.0053
Groundnuts in shell	0.040	0.0042
Maize	0.014	0.0029
Millet	0.015	0.0030
Oil palm fruit	0.015	0.0031
Potatoes	0.003	0.0005
Pulses, total	0.035	0.0025
Rapeseed	0.035	0.0056
Rice, paddy	0.013	0.0025
Rye (other cereals)	0.016	0.0031
Sorghum	0.015	0.0030
Soybeans	0.035	0.0050
Sugar beets	0.002	0.0004
Sugar cane	0.002	0.0004
Sunflower seed	0.034	0.0045
Wheat	0.019	0.0034
Other crops	0.009	0.0016

Results & discussion

Hydrology

For the 1980–2001 period, the modelled monthly water fluxes fit well to the observed data at the monitoring station at Lobith, as shown in Fig. 6, (Nash and Sutcliffe, 1970; coefficient of model efficiency $E = 0.76$). Furthermore, the modelled annual discharge over the same period (7.36×10^{10} m^3 y^{-1}) is close to the observed discharge (7.54×10^{10} m^3 y^{-1}). The seasonal trend is well represented, although for some years discharge peaks are not always predicted. The modelled discharge of the upstream stations also shows good agreement with the observed data. The minimum modelled monthly discharge at Lobith is 1144 m^3 s^{-1} (observed minimum of 874 m^3 s^{-1}). The maximum modelled discharge of 5206 m^3 s^{-1} is closer to the observed maximum 5453 m^3 s^{-1}. Despite a much coarser climate input dataset was used, the model efficiency of the PCRglobWB model is comparable to that obtained by Kwadijk and Middelkoop (1994). Therefore, we conclude that the ERA40 data is suitable for basin scale hydrology modelling, and provides a consistent dataset for inter-basin comparison.

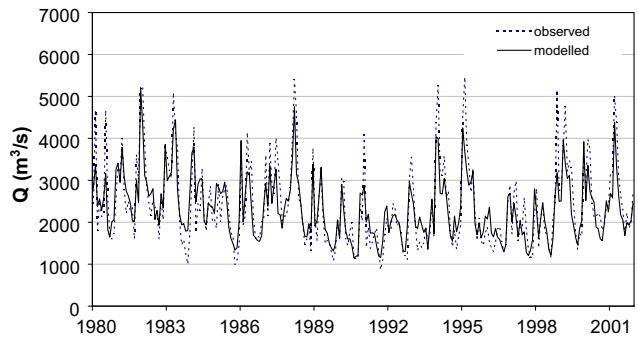

Fig. 6. Monthly observed and modelled discharge ($m^3 s^{-1}$) at Lobith (Rhine) between 1980 and 2001.

Sediment

The model results for the monthly suspended sediment (TSS) load estimated for the Rhine basin upstream from Lobith (Fig. 7) has a model efficiency of $E = 0.23$. The calibrated modelled annual TSS load passing Lobith between 1984 and 2000 (2.94×10^6 t y^{-1}) was close to the observed load (2.82×10^6 t y^{-1}). The observed monthly TSS load during the period for which measurement data was available (1984–1991 and 1994–2000) ranged between 29 and 1339 kg s^{-1}. The modelled load for the same period had a slightly narrower range of 71–1322 kg s^{-1}. Nevertheless, most sediment flux peaks and the range of monthly loads were simulated reasonably well.

Nutrients

Inputs and losses

The largest absolute difference in net emission estimates between the RHIN and GLOB dataset is observed for nutrient loss via crops harvest (yield) and N input to agricultural areas from manure application (Table 7). The relative difference is highest for other diffuse emission, mainly emission from households not connected to sewerage systems. Overall, the GLOB dataset overestimates basin nutrient loading compared to the RHIN dataset with 33% and 17%, for N and P, respectively.

The RHIN and GLOB datasets used for this study differ in spatial resolution. This inevitably led to generalizations in allocation (district versus country level) and model parameters for emission gains or losses (e.g. excretion rates, crop nutrient content, WWTP efficiencies). The GLOB dataset uses global estimates that in reality may differ from (sub)basin to (sub)basin. This may have caused uncertainties in model input and, consequently, relatively large uncertainties in the model output. Other inconsistencies may have arisen from the rescaling of few maps to the base years 1992/1993.

Although the RHIN dataset probably better allocates and quantifies real nutrient inputs and losses, both the RHIN and GLOB datasets may contain errors. Table 7 lists the nutrient loading per emission type summed for the entire basin. It clearly shows that most of the uncertainty in nutrient emission estimation lies in the direct inputs from point sources including industries; an often used approach at global scale is to relate human nutrient emission to GDP (gross domestic product). In this study, this approach was also pursued for the GLOB dataset. The relationship between human nutrient emission to GDP may not be adequate for all individual river basins. Furthermore, it is debatable whether nutrient emission from population not connected to sewerage directly enters surface waters (as was assumed in this study) or is emitted as a diffuse source.

The relative large difference in manure application may arise from uncertainty in livestock numbers, but also from different excretion rates used in the datasets. The relative underestimation of N removal in crop yield by the GLOB dataset is likely due to variation in crop nutrient contents used. Still, the difference in estimation of the net (direct or diffuse) nutrient emission to the aquatic system between the RHIN and GLOB dataset seems reasonable given the large difference in detail of both datasets, and lies well within the range of estimation errors that may arise from uncertainties in the emission rate values.

N fluxes

Fig. 8 shows the modelled and observed TN loads at Lobith between 1990 and 2000. For the RHIN dataset, the modelled TN loads fit generally well to the observed loads ($E = 0.50$) (Fig. 9). The GLOB dataset has a lower efficiency of $E = 0.12$ (Fig. 10). For the modelled period (1990–2000) minimum and maximum observed TN loads at

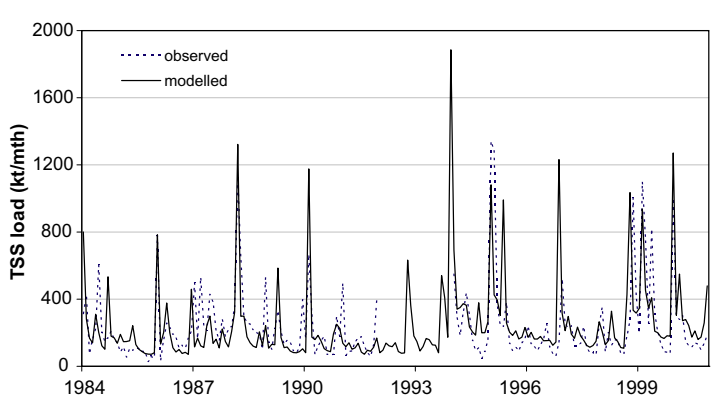

Fig. 7. Monthly observed and modelled sediment load (kt mth^{-1}) at Lobith (Rhine) between 1984 and 2000.

Table 7
Comparison of nutrient emission for 1992 as estimated by the RHIN and GLOB dataset for the entire Rhine basin.

	N inputs (+)/losses (−) (10^6 kg y^{-1})		P inputs (+)/losses (−) (10^6 kg y^{-1})	
	Dataset		Dataset	
	RHIN	GLOB	RHIN	GLOB
Diffuse inputs (or loss) to the land				
Fertilizer	99.8	103.5	16.0	16.0
Manure	81.7	102.9	19.5	18.5
Yield loss	−117.2	−102.3	−22.6	−18.8
Other diffuse input	1.8	4.4	0.2	0.6
Total diffuse inputs	66.0	108.6	13.1	16.3
Point inputs to surface waters				
Point sources	32.3	22.3	3.0	2.3

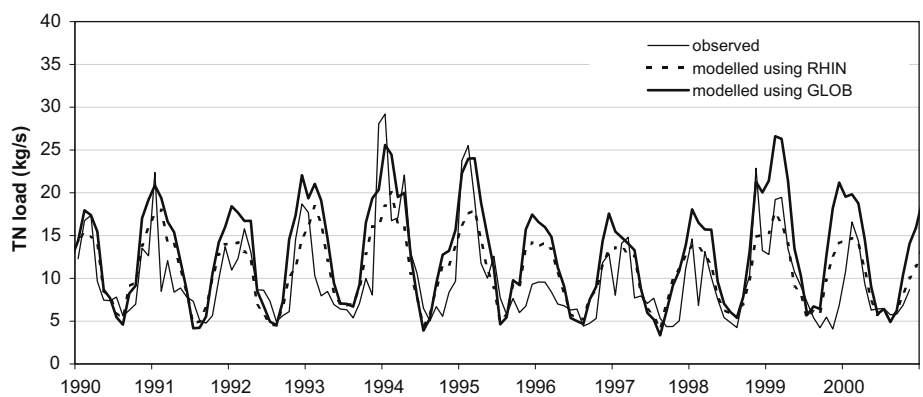

Fig. 8. Total N load (kg s^{-1}) at Lobith (Rhine) between 1990 and 2000.

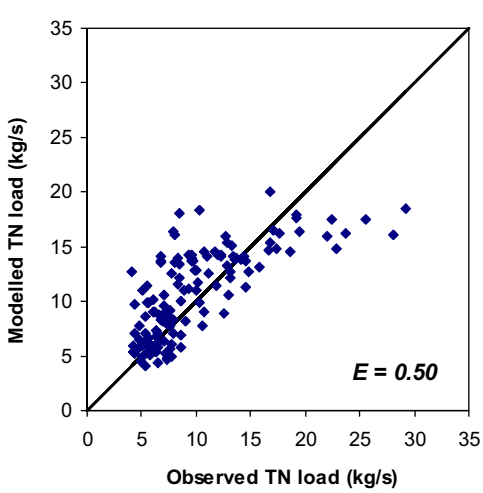

Fig. 9. Observed versus modelled total N load (kg s^{-1}) using the RHIN dataset.

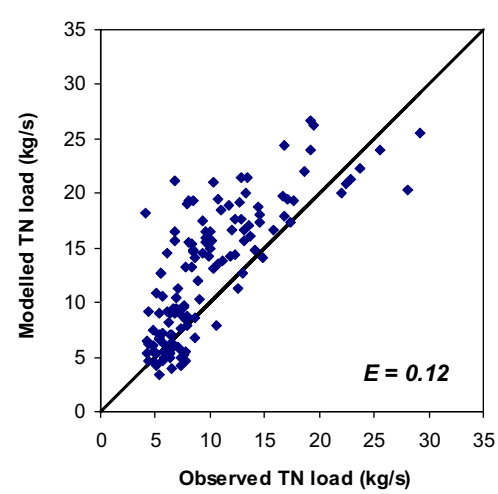

Fig. 10. Observed versus modelled total N load (kg s^{-1}) using the GLOB dataset.

Lobith are 4.1 kg s^{-1} and 29.2 kg s^{-1}, respectively. Modelled loads range between 4.1 and 20.0 kg s^{-1} for the RHIN dataset and 3.3–26.6 kg s^{-1} for the GLOB dataset. The model results for TN show a pronounced seasonal variation in line with the observed high TN loads in winter and lowest observed TN loads in the summer months (Fig. 8). Also variation between years with wet years showing higher nutrient loads is adequately simulated by RiNUX. Total N loads for the whole period add up to 3.41×10^5 t (observed), 3.72×10^5 t (RHIN), and 4.46×10^5 t (GLOB). Groundwater is a large supplier of nitrates contributing more than half of the TN load observed at Lobith. The nitrogen load at Lobith is satisfactory calculated by the RiNUX model when RHIN is used as input, generating the mean long-term TN load as well as the seasonal variability. Some years do not show a perfect fit, which can be partly attributed to the hydrological flux input that also shows an underestimation in peak discharge. The GLOB dataset slightly overestimates nutrient loads, which is probably largely due to an overestimation of nutrient emission (Table 7).

P fluxes

Fig. 11 shows the modelled and observed TP loads at Lobith between 1974 and 2001. The model efficiency for the P fluxes is $E = 0.47$ for the RHIN dataset (Fig. 12) and $E = 0.36$ for the GLOB dataset (Fig. 13). The minimum TP loads for the 1974–2001 period are 0.2 kg s^{-1} (observed), 0.7 kg s^{-1} (RHIN), and 0.4 kg s^{-1} (GLOB). For the same period, the maximum TP loads are 3.2 kg s^{-1} (ob-

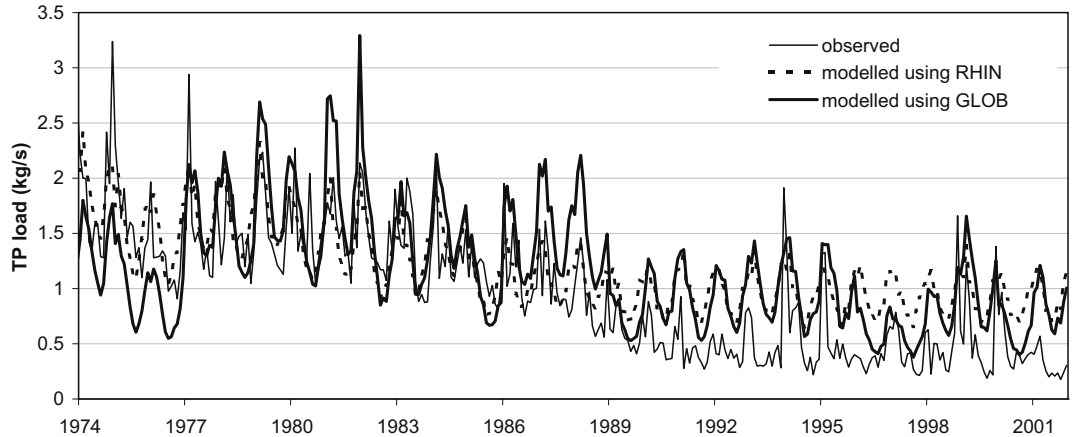

Fig. 11. Total P load (kg s^{-1}) at Lobith (Rhine) between 1974 and 2001.

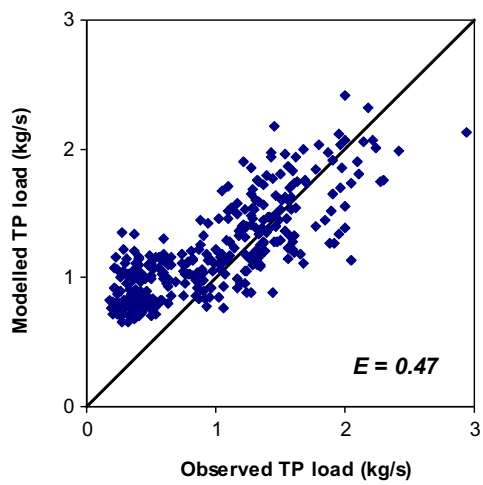

Fig. 12. Observed versus modelled total P load (kg s^{-1}) using the RHIN dataset.

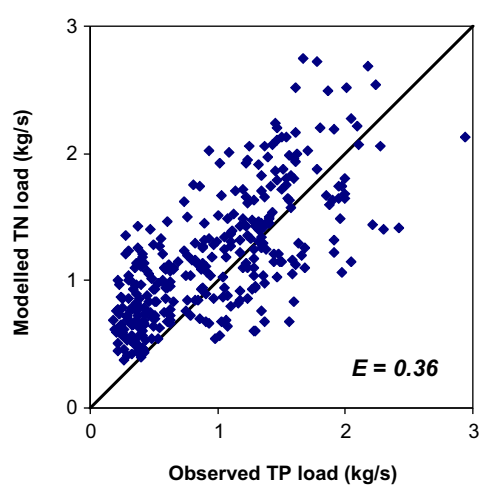

Fig. 13. Observed versus modelled total P load (kg s^{-1}) using the GLOB dataset.

served), 2.4 kg s^{-1} (RHIN), and 3.3 kg s^{-1} (GLOB). As for TN, the seasonal variation of TP loads is well simulated (Fig. 11). The total observed P flux between 1974 and 2001 is 8.55×10^5 t. Using the RHIN dataset, the TP flux is estimated at 10.57×10^5 t versus 10.42×10^5 t using the GLOB dataset. Both datasets overestimate the TP load from the 90s onwards. If the total P flux between 1974 and 1990 is considered, much better results are obtained; estimates amount to 6.95×10^5 t (RHIN) and 7.14×10^5 t (GLOB) versus the total P flux of 6.71×10^5 t observed at Lobith.

The shift from high loads during the 80s to lower loads in the 90s is reasonably represented by the model, although the observed trend is more pronounced. The overestimation of P loads after 1990 is probably due to an overestimated contribution from households. Tertiary treatment and the reduced use of P containing washing detergents has caused a decline of P emissions since the beginning of the 1990s (Van der Perk, 2006). However, the introduction of tertiary treatment was not reflected in the GLOB dataset because a constant fixed ratio between the N and P removal efficiency coefficient was used. This has lead to an underestimation of the P removal efficiency and a consequent overestimation of direct P input to surface waters. Likewise, the last period of the RHIN dataset (1990–1995) may not represent the WWTP removal efficiency for P correctly.

Conclusions & perspectives

This paper presented the newly developed RiNUX model to simulate and predict monthly N and P fluxes in large river basins. The strength of the model lies in the fact that it takes seasonal variation in nutrient loads and speciation between dissolved nutrient forms and particulate forms originating from surface erosion on hillslopes into account. This makes the RiNUX model a powerful tool to simulate within-basin processes at a large scale.

This study has shown that global datasets can be satisfactorily used in seasonal nutrient flux modelling at the larger basin scale. Still improvements can be achieved when the input maps gain more detail.

The RiNUX model shows reasonably good results for both TN and TP loads. Results from the detailed RHIN dataset are slightly better than for the global, less detailed, GLOB dataset. The main cause for the observed difference in simulated nutrient loads is the relative overestimation of N and P surplus at the soil surface. Seasonal variability is well represented, although winter loads are generally overestimated. With improved global input (new datasets or calibration against regional data) better results can be achieved. The GLOB dataset is an incipient form of such a dataset, providing a consistent parameterization for the comparison between the different large basins. This facilitates the understanding of nutrient transfer under different (climatic) conditions and varying pressures (emission intensity), thereby enabling global change impact assessment.

In the coming years, the global datasets are expected to be extended and improved and become more readily available, which provides an excellent perspective for application of the RiNUX model to other large river basins. Although the application of the RiNUX model would be straightforward if the GLOB dataset or future improved datasets are used, it is likely that some further adjustments to the RiNUX model may be necessary for application to river basins. These adjustments include (1) a coarser spatial resolution due to computational restrictions if larger basins than the Rhine are modelled, (2) water withdrawal assessment in basins where water redistribution is important, and (3) additional calibration of processes like snow melt and temperature dependent within-stream nutrient losses for arctic and tropical river systems.

Acknowledgements

The work on this project was made possible by financial support from Utrecht University (High Potential project G-NUX). The authors would like to thank Marcel de Wit for providing the RHIN dataset, and Lex Bouwman, Gerard van Drecht (MNP – The Netherlands) and Jens Hartmann (Darmstadt University – Germany) for providing valuable insight and data used to construct the GLOB dataset.

References

Ahad, J.M.E., Ganeshram, R.S., Spencer, R.G.M., Uher, G., Upstill-Goddard, R.C., Cowie, G.L., 2006. Evaluating the sources and fate of anthropogenic dissolved inorganic nitrogen (DIN) in two contrasting North Sea estuaries. Science of the Total Environment 372 (1), 317–333.

Alcamo, J., Döll, P., Henrichs, T., Kaspar, F., Lehner, B., Rösch, T., Siebert, S., 2003. Development and testing of the WaterGAP 2 global model of water use and availability. Hydrological Sciences Journal 48 (3), 317–338.

Andersson, L., Rosberg, J., Pers, B.C., Olsson, J., Arheimer, B., 2005. Estimating catchment nutrient flow with the HBV-NP model: sensitivity to input data. Ambio: A Journal of the Human Environment 34 (7), 521–532.

Arheimer, B., Brandt, M., 1998. Modelling nitrogen transport and retention in the catchments of southern Sweden. Ambio 27 (6), 471–480.

Asselman, N.E.M., 2000. Fitting and interpretation of sediment rating curves. Journal of Hydrology 234 (3–4), 228–248.

Asselman, N.E.M., Middelkoop, H., van Dijk, P.M., 2003. The impact of changes in climate and land use on soil erosion, transport and deposition of suspended sediment in the River Rhine. Hydrological Processes 17 (16), 3225–3244.

Batjes, N.H., 1996. Total carbon and nitrogen in the soils of the world. European Journal of Soil Science 47 (2), 151–163.

Behrendt, H., 1996. Inventories of point and diffuse sources and estimated nutrient loads – a comparison for different river basins in Central Europe. Water Science and Technology 33 (4–5), 99–107.

Behrendt, H., Huber, P., Kornmilch, M., Opitz, D., Schmoll, O., Scholz, G., Uebe, R., 2000. Nutrient emissions into river basins of Germany. UBA-Texte 23/00, 261 pp. (Berlin).

Bergström, S., 1995. The HBV Model. In: Singh, V.P. (Ed.), Computer Models of Watershed Hydrology. Water Resources Publications, Colorado, pp. 443-476.

Beusen, A.H.W., Dekkers, A.L.M., Bouwman, A.F., Ludwig, W., Harrison, J., 2005. Estimation of global river transport of sediments and associated particulate C, N, and P. Global Biogeochemical Cycles 19 (4), GB4S05. doi:10.1029/2005GB002453.

BfG, 2007. Bundesanstalt für Gewässerkunde, Koblenz. <http://www.iksr.org/>.

Billen, G., Garnier, J., Hanset, P., 1994. Modelling phytoplankton development in whole drainage networks: the 'Riverstrahler' model applied to the Seine river system. Hydrobiologia 289 (1), 119–137.

Bouwman, A.F., Boumans, L.J.M., Batjes, N.H., 2002. Estimation of global NH_3 volatilization loss from synthetic fertilizers and animal manure applied to arable lands and grasslands. Global Biogeochemical Cycles 16 (4), 1024. doi:10.1029/2000GB001389.

Bouwman, A.F., Van Drecht, G., Van der Hoek, K.W., 2005. Global and regional surface nitrogen balances in intensive agricultural production systems for the period 1970–2030. Pedosphere 15 (2), 137–155.

Caraco, N.F., Cole, J.J., 1999. Human impact on nitrate export: an analysis using major world rivers. Ambio 28 (2), 167–170.

CGIAR-CSI, 2004. Void-filled seamless SRTM data V1. International Centre for Tropical Agriculture (CIAT). The CGIAR-CSI SRTM 90m database. <http://srtm.csi.cgiar.org>.

CIESIN, 2005. Center for International Earth Science Information Network, Columbia University; and Centro Internacional de Agricultura Tropical (CIAT). Gridded population of the world version 3 (GPWv3): population grids. Socioeconomic Data and Applications Center (SEDAC), Columbia University, Palisades, NY. <http://sedac.ciesin.columbia.edu/gpw>.

Cleveland, C.C., Townsend, A.R., Schimel, D.S., Fisher, H., Howarth, R.W., Hedin, L.O., Perakis, S.S., Latty, E.F., Von Fischer, J.C., Elseroad, A., Wasson, M.F., 1999. Global patterns of terrestrial biological nitrogen (N_2) fixation in natural ecosystems. Global Biogeochemical Cycles 13 (2), 623–645.

Crossland, C.J., Kremer, H.H., Lindeboom, H.J., Crossland, J.I.M., Tissier, M.D.A.L., 2005. Coastal Fluxes in the Anthropocene: The Land–Ocean Interactions in the Coastal Zone Project of the International Geosphere–Biosphere Programme. Springer, Berlin. 231 pp.

De Fries, R.S., Hansen, M., Townshend, J.R.G., Janetos, A.C., Loveland, T.R., 1999. Global 1 km data set of percent tree cover derived from remote sensing. Global Land Cover Facility, University of Maryland Institute for Advanced Computer Studies, College Park, Maryland, USA. <http://glcf.umiacs.umd.edu>.

De Wit, M.J.M., 1999. Nutrient fluxes in the Rhine and Elbe basins. Nederlands Geografische Studies 259 Thesis, Universiteit Utrecht, Utrecht, 163 pp.

De Wit, M.J.M., 2001. Nutrient fluxes at the river basin scale. I: the PolFlow model. Hydrological Processes 15 (5), 743–759.

Dentener, F.J., 2006. Global maps of atmospheric nitrogen deposition, 1860, 1993, and 2050. Data set. Oak Ridge National Laboratory Distributed Active Archive Center, Oak Ridge, Tennessee, USA. <http://daac.ornl.gov/>.

Doomen, A.M.C., Wijma, E., Zwolsman, J.J.G., Middelkoop, H., 2008. Predicting suspended sediment concentrations in the Meuse river using a supply-based rating curve. Hydrological Processes 22 (12), 1846–1856.

Dürr, H.H., Meybeck, M., Dürr, S.H., 2005. Lithologic composition of the earth's continental surfaces derived from a new digital map emphasizing riverine material transfer. Global Biogeochemical Cycles 19, GB4S10. doi:10.1029/2005GB002515.

FAO, 2002. Fertilizer Use by Crop, fifth ed. FAO, Rome. 45pp.

FAO, 2007. (GLi(GLiPHA) Gridded Livestock of the World 2007 by G.R.W. Wint and T.P. Robinson. FAO, Rome. 131pp. <http://www.fao.org/geonetwork>.

FAOSTAT database collection, 2006. Food and Agriculture Organization (FAO) of the UN, Rome. <http://www.apps.fao.org>.

FAO-UNESCO, 1995. The Digital Soil Map of the World and Derived Soil Properties. Land and Water Digital Media Series, vol. 1. FAO, Rome (CD-ROM).

GRDC, 2007. Global Runoff Data Centre in the Federal Institute of Hydrology (BfG), Koblenz. <http://grdc.bafg.de>.

GTOPO30/Hydro1k, 1996. US Geological Survey, Center for Earth Resources Observation and Science (EROS). USGS/EROS, Sioux Falls, SD, USA. <http://eros.usgs.gov/>.

Holland, E.A., Braswell, B.H., Sulzman, J., Lamarque, J.-F., 2004. Nitrogen deposition onto the United States and Western Europe. Oak Ridge National Laboratory Distributed Active Archive Center, Oak Ridge, Tennessee, USA. <http://www.daac.ornl.gov>.

IFPRI, 2002. Land use-land cover map of the world. Pilot analysis of global ecosystems (PAGE): agroecosystems, 2000, 2005. World Resources Institute and the International Food Policy Research Institute (datasets), Washington, DC. <http://www.fao.org/geonetwork/>.

IKSR, 2004. Zahlentafeln – Der Physikalisch-Chemischen Untersuchungen des Rheinwassers und des Schwebstoffs. Bundesanstalt für Gewässerkunde, Koblenz. <http://had.bafg.de:8080/iksr-zt/>.

Johnes, P.J., 2007. Uncertainties in annual riverine phosphorus load estimation: impact of load estimation methodology, sampling frequency, baseflow index and catchment population density. Journal of Hydrology 332 (1–2), 241–258.

Kristensen, P., Fribourg-Blanc, B., Nixon, S., Isoard, S., 2005. Outlooks on nutrient discharges in Europe from urban waste water treatment plants. EEA European Topic Centre on Water, Copenhagen.

Kwadijk, J., Middelkoop, H., 1994. Estimation of impact of climate change on the peak discharge probability of the river Rhine. Climatic Change 27 (2), 199–224.

LandScan™ Global population database, 2002. Oak Ridge National Laboratory, Oak Ridge, TN. <http://www.ornl.gov/landscan/>.

Lartiges, B.S., Deneux-Mustin, S., Villemin, G., Mustin, C., Barres, O., Chamerois, M., Gerard, B., Babut, M., 2001. Composition, structure and size distribution of suspended particulates from the Rhine River. Water Research 35 (3), 808–816.

Leff, B., Ramankutty, N., Foley, J.A., 2004. Geographic distribution of major crops across the world. Global Biogeochemical Cycles 18, GB1009. doi:10.1029/2003GB002108.

McGuire, K.J., McDonnell, J.J., Weiler, M., Kendall, C., McGlynn, B.L., Welker, J.M., Seibert, J., 2005. The role of topography on catchment-scale water residence time. Water Resources Research 41, W05002. doi:10.1029/2004WR003657.

Meybeck, M., 1993. C, N, P and S in Rivers: from sources to global inputs. In: Wollast, R., Mackenzie, F.T., Chou, L. (Eds.), Interaction of C, N, P, and S Biogeochemical Cycles and Global Change. Springer–Verlag, Berlin, pp. 163–193.

Middelkoop, H., Van Haselen, C.O.G., 1999. Twice a River: Rhine and Meuse in the Netherlands& RIZA. Institute for Inland Water Management and Waste Water Treatment, Arnhem. p. 127.

Morgan, R.P.C., 2001. A simple approach to soil loss prediction: a revised Morgan–Morgan–Finney model. Catena 44 (4), 305–322.

Nash, J.E., Sutcliffe, J.V., 1970. River flow forecasting through conceptual models part I – a discussion of principles. Journal of Hydrology 10 (3), 282–290.

Newman, E.I., 1995. Phosphorus inputs to terrestrial ecosystems. The Journal of Ecology 83 (4), 713–726.

Owens, P.N. and Deeks, L.K., 2004. The role of soil phosphorus in controlling sediment-associated phosphorus transfers in river catchments. In: Golosov, V., Belyaev, V., Walling, D.E. (Eds.), Sediment Transfer through the Fluvial System. IAHS Publication 288. IAHS Press, Wallingford, pp. 444-450.

Rabalais, N., Turner, R.E., Dortch, Q., Justic, D., Bierman, V., Wiseman, W., 2002. Nutrient-enhanced productivity in the northern Gulf of Mexico: past, present and future. Hydrobiologia 475–476 (1), 39–63.

Schreiber, H., Constantinescu, L.T., Cvitanic, I., Drumea, D., Jabucar, D., Juran, S., Pataki, B., Snishko, S., Zessner, M., Behrendt, H., 2003. Harmonised Inventory of Point and Diffuse Emission of Nitrogen and Phosphorus for a Transboundary River Basin. UBA-FB, Leibniz – Institute of Freshwater Ecology and Inland Fisheries, Berlin.

Seitzinger, S.P., Kroeze, C., Bouwman, A.F., Caraco, N., Dentener, F., Stylesa, R.V., 2002. Global patterns of dissolved inorganic and particulate nitrogen inputs to coastal systems: recent conditions and future projections. Estuaries 25 (4), 640–655.

Seitzinger, S.P., Harrison, J.A., Dumont, E., Beusen, A.H.W., Bouwman, A.F., 2005. Sources and delivery of carbon, nitrogen, and phosphorus to the coastal zone: an overview of Global Nutrient Export from Watersheds (NEWS) models and their application. Global Biogeochemical Cycles 19 (4), GB4S01. doi:10.1029/2005GB002606.

Smil, V., 1999. Nitrogen in crop production: an account of global flows. Global Biogeochemical Cycles 13, 647–662.

Syvitski, J.P.M., Peckham, S.D., Hilberman, R., Mulder, T., 2003. Predicting the terrestrial flux of sediment to the global ocean: a planetary perspective. Sedimentary Geology 162 (1–2), 5–24.

Syvitski, J.P.M., Vörösmarty, C.J., Kettner, A.J., Green, P., 2005. Impact of humans on the flux of terrestrial sediment to the global coastal ocean. Science 308, 376–380.

Tappin, A.D., 2002. An examination of the fluxes of nitrogen and phosphorus in temperate and tropical estuaries: current estimates and uncertainties. Estuarine, Coastal and Shelf Science 55 (6), 885–901.

Uppala, S.M., Kallberg, P.W., Simmons, A.J., Andrae, U., Bechtold, V.D., Fiorino, M., Gibson, J.K., Haseler, J., Hernandez, A., Kelly, G.A., Li, X., Onogi, K., Saarinen, S., Sokka, N., Allan, R.P., Andersson, E., Arpe, K., Balmaseda, M.A., Beljaars, A.C.M., Van De Berg, L., Bidlot, J., Bormann, N., Caires, S., Chevallier, F., Dethof, A., Dragosavac, M., Fisher, M., Fuentes, M., Hagemann, S., Holm, E., Hoskins, B.J., Isaksen, L., Janssen, P.A.E.M., Jenne, R., McNally, A.P., Mahfouf, J.F., Morcrette, J.J., Rayner, N.A., Saunders, R.W., Simon, P., Sterl, A., Trenberth, K.E., Untch, A., Vasiljevic, D., Viterbo, P., Woollen, J., 2005. The ERA-40 re-analysis. Quarterly Journal of the Royal Meteorological Society 131, 2961–3012.

Van Beek, L.P.H., Bierkens, M.F.P., 2006. Base flow regionalization and calibration in a global hydrological model, AGU General Assembly, San Francisco, USA, 11–15 December 2006.

Van der Perk, M., 2006. Soil and water contamination: from molecular to catchment scale. Taylor and Francis/Balkema, Leiden, 389 p.

Van Drecht, G., Bouwman, A.F., Knoop, J.M., Beusen, A.H.W., Meinardi, C.R., 2003. Global modeling of the fate of nitrogen from point and nonpoint sources in soils, groundwater, and surface water. Global Biogeochemical Cycles 17 (4), 1115.

Venterink, H.O., Wiegman, F., Van der Lee, G.E.M., Vermaat, J.E., 2003. Role of active floodplains for nutrient retention in the River Rhine. Journal of Environmental Quality 32 (4), 1430–1435.

Waterbase, 2008. RWS WD (Rijkswaterstaat Centre for Water Management), Lelystad. <http://www.waterbase.nl>.

Wesseling, C.G., Karssenberg, D.J., Burrough, P.A., Van Deursen, W.P.A., 1996. Integrating dynamic environmental models in GIS: the development of a dynamic modelling language. Transactions in GIS 1 (1), 40–48.

Wollheim, W.M., Vörösmarty, C.J., Bouwman, A.F., Green, P., Harrison, J., Linder, E., Peterson, B.J., Seitzinger, S.P., Syvitski, J.P.M., 2008. Global N removal by freshwater aquatic systems using a spatially distributed, within-basin approach. Global Biogeochemical Cycles 22, GB2026.